Research Square

Preprints are preliminary reports that have not undergone peer review.
They should not be considered conclusive, used to inform clinical practice,
or referenced by the media as validated information.

Automatic Extraction of Welding Trajectories for V-Groove Welds Based on 3-D Active Vision Imaging

Jingjing Lou
Shenyang Jianzhu University
Yuanhan Li
liyunhan@zjhzu.edu.cn
Huzhou College
Liangliang Sun
Shenyang Jianzhu University
Chuan Ye
Southwest Petroleum University
Yuancheng Zhu
Huzhou College

Research Article

Keywords: Active Vision Imaging, Feature Fusion, Stripe Segmentation, Centerline Extraction, Welding Trajectory

Posted Date: August 10th, 2026

DOI: https://doi.org/10.21203/rs.3.rs-7902738/v1

License: This work is licensed under a Creative Commons Attribution 4.0 International License.
Read Full License

Additional Declarations: No competing interests reported.

Automatic Extraction of Welding Trajectories for V-Groove Welds Based on 3-D Active Vision Imaging

Jingjing Lou[1,2], Yunhan Li[3,*], Liangliang Sun[1,4], Chuan Ye[5], Yuancheng Zhu[3]

[1]Shenyang Jianzhu University, Shenyang, 110168, China
[2]Taizhou Vocational and Technical College, Taizhou, 318000, China
[3] Huzhou College, Huzhou 313000, China
[4] Northeastern University, Qinghuangdao 066004, China
[5] Southwest Petroleum University, Nanchong, 637000, China
*Correspondence: liyunhan@zjhzu.edu.cn; Tel.: +86-130-59969688

Abstract: To automatically extract welding trajectories for planar welds on reflective materials, this paper proposes a three-dimensional active vision-based welding trajectory extraction methodology that is based on the fusion of features. First, to accurately segment the laser stripes at the weld seam, a saliency feature fusion-based laser stripe segmentation model (SFF_LSM) has been developed. The SFF_LSM model effectively suppresses background interference features, accurately segmenting the general features of the laser stripe distribution along the weld seam. Next, the gray-gravity algorithm with secondary smoothing is employed to extract the center of the laser stripe. Finally, the point cloud data at the weld seam is filtered, and the least squares fitting algorithm is employed to extract the welding trajectory automatically. The results of the experiment demonstrate that the proposed method is an effective means of overcoming the interference caused by reflections, with the maximum fitting errors of the weld seam welding trajectory being 0.51 mm in the X direction, 0.40 mm in the Y direction, and 0.29 mm in the Z direction.

Key words: Active Vision Imaging, Feature Fusion, Stripe Segmentation, Centerline Extraction, Welding Trajectory

1 Introduction

The development of welding technology has become an essential part of the manufacturing industry. Manual welding still dominates most production processes. However, with rising labor costs and the complexity and hazards of the welding environment, the development of automatic welding technology has become an urgent task [1, 2]. Traditional welding robots

require precise position teaching or offline programming to execute predetermined trajectories, resulting in low production efficiency. Line-structured light 3D measurement systems are widely used in weld seam feature recognition and tracking due to their advantages of speed, stability, non-contact operation, and ability to capture detailed information [3-5]. For welding robots operating in unstructured environments, the challenge of extracting welding trajectories amidst interference caused by lighting variations and diverse workpiece materials has become a key research focus.

In recent years, researchers both domestically and internationally have extensively studied feature extraction methods for weld seams. Lü et al. [6] used a fixed threshold method to segment different types of weld seams to extract their features. However, this method is susceptible to noise interference. Sung et al. [7] proposed a high-precision structured light weld seam tracking system, which uses filtering algorithms to eliminate residual laser stripes and enhance the laser stripes for segmentation to detect weld seams. He et al. [8] used a novel saliency-based visual attention model for the purpose of detecting weld seam contours, which exhibited strong anti-interference capabilities. Banafian et al. [9] proposed a structured light weld system for the tracking of seams that employs laser and stereo vision, using an enhanced edge detection algorithm to determine weld seam parameters. However this method is prone to errors under reflective characteristics. Fang et al. [10] performed scan imaging on the weld seam to collect feature points, and then combined the least squares algorithm with the RANSAC method to detect and smooth the weld seam from the feature points. Lu et al. [11] tackled the interference caused by arc light and spatter noise by using deep learning for feature segmentation to extract weld seam features, achieving high resistance to environmental disturbances. Li et al. [12] put forth a novel approach to extract the centerline for tracking weld seam features in the presence of noise interference. They employed the least squares method for curve fitting to obtain the weld seam tracking path, demonstrating remarkable adaptability. Ye et al. [13] studied 3-D imaging of reflective workpieces and used deep learning models for effective segmentation, demonstrating strong robustness. Zhang et al. [14] proposed a 3D-based planar weld extraction method that employs the RANSAC iterative segmentation technique and uses least squares to extract weld features. Zhang et al. [15] presented methodology for the extraction of corners from workpieces in three-dimensional visual welding. This methodology entails the construction of a feature space of the workpiece point cloud through the utilization of the LOBB feature descriptor, with the objective of enhancing the robustness of feature clustering through nonlinear activation. Ultimately, this results in the design of a hierarchical clustering method based on K-means, which is employed to achieve key point extraction.

Although many researchers have extensively studied weld seam feature extraction methods, further research is required to address the impact of environmental light interference. uneven surface reflection of weldments, and laser scattering during the welding process. This paper

analyzes the characteristics of laser stripe images and adopts a saliency feature fusion method to achieve precise segmentation of the stripes. Secondly, a gray-gravity algorithm with secondary smoothing is employed for extracting the center of the laser stripes. Finally, the least squares method is combined to fit the weld seam trajectory from the 3D feature points. Experimental results demonstrate that the proposed algorithm is effective in mitigating interference from reflections and background noise, with the extracted weld seam trajectory exhibiting a maximum error of less than 0.51 mm. This lays a theoretical and practical foundation for the feature extraction and tracking of planar weld seams in complex scenes.

2 Basic principles and method design

2.1 Saliency feature fusion-based precise segmentation of V-Groove

This paper employs an active vision imaging method, which requires projecting high-brightness laser stripes onto the welding workpiece, making it even more challenging to measure materials with reflective properties. To achieve segmentation of the weld seam, this paper adopts a Saliency Feature Fusion-based V-Groove Segmentation Model (SFF-LSM). The algorithm flowchart is shown in Fig.1.

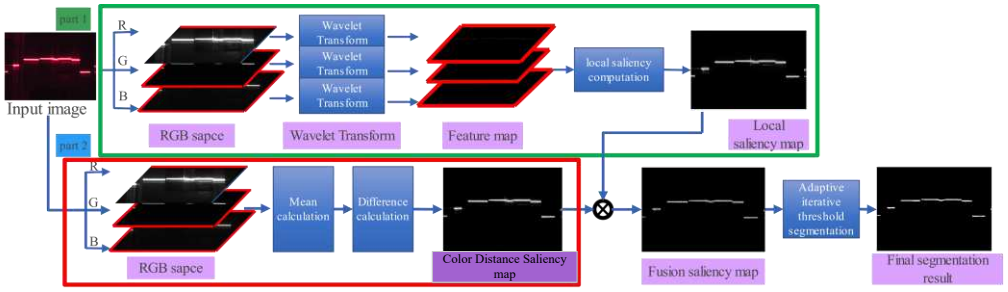


Fig. 1 SFF-LSM flow chart

Firstly, to address background reflection interference, the average value of the three-channel images in the RGB color space is calculated separately. The RGB channel images are then subtracted by the mean and normalized to obtain a color distance saliency map. The color distance saliency map is effective in minimizing the influence of background reflections on the laser stripes along the weld seam. The function expression for the colour distance saliency map is as follows:

$$S_I = | I_c(x,y) - \bar{I}_c |^2 \tag{1}$$

where $I_c(x,y)$ signifies the image that is to be input, $\bar{I}_c$ represents the average of the input picture, and c is the color channel of the input image, $c \in \{R,G,B\}$.

Secondly, to obtain effective features at the weld seam, the RGB color channels are separately decomposed using 2D wavelet decomposition[16]. Considering the size and

efficiency of the filtering, the db5 filter is used for the wavelet decomposition. The functional expression is as follows:

$$\left[A_N^c, H_s^c, V_s^c, D_s^c\right] = WT_N(f^c(x,y)) \tag{2}$$

where $WT_N(\cdot)$ is the wavelet decomposition function at level *N*, *N* is the maximum scale number in the decomposition process, and $s \in \{1,\cdots,N\}$ is the resolution index. $f^c(x,y)$ is the input picture, c denotes the color channel of the input image, $c \in \{R,G,B\}$ .The value A_N^c represents the approximation output at the lowest resolution for each channel. The wavelet coefficients H_s^c , V_s^c , and D_s^c correspond to different decomposition levels in the horizontal, vertical, and diagonal directions, respectively, capturing the detailed features of the image across various levels of decomposition.

The feature map at this level can be obtained by reconstructing the image using inverse wavelet transform. The functional expression is as follows:

$$f_s^c(x,y) = (IWT_s(H_s^c, V_s^c, D_s^c))^2 \cdot p^{-1} \tag{3}$$

where $f_s^c(x,y)$ is the feature map obtained by decomposing and reconstructing each color channel of the image at level s, $IWT_s(\cdot)$ is the inverse wavelet transform reconstruction function. The parameter p serves as a constraint factor because the RGB channel range of the input image spans from [0-255], potentially causing a wide distribution of pixel values in the calculated feature map., The feature map can be effectively constrained by selecting an appropriate value for p . In this paper, p is set to $p = 10^4$.

Local saliency features can effectively focus on weld laser stripe characteristics, capturing the stripe information more accurately. In this paper, the feature maps of each layer are linearly fused. The functional expression is in the following way:

$$S_L(x,y) = (\sum_{s=1}^{N} \arg\max(f_s^R(x,y), f_s^G(x,y), f_s^B(x,y))) * g \tag{4}$$

where $f_s^R(x,y)$, $f_s^G(x,y)$, and $f_s^B(x,y)$ represent the feature maps for the RGB channels, while $S_L(x,y)$ denotes the local saliency map. The symbol *g* refers to a 5×5 2D Gaussian low-pass filter.

Finally, the color distance saliency map S_I and the local saliency map S_L are fused to suppress background noise and reflections based on their complementary advantages. The functional expression is as follows:

$$S = S_I * S_L \tag{5}$$

Iterative thresholding is a commonly applied technique in image segmentation. It determines the segmentation threshold of the pixels through iterative calculations. Firstly, the maximum value of the grey scale Z_{max} and the minimum value of the grey scale value Z_{min} of the fused saliency map *S* are calculated. Therefore, the initial threshold $T_0 = \{T_k \mid k = 0\}$ is expressed as:

$$T_0 = \frac{Z_{\max} + Z_{\min}}{2} \tag{6}$$

Next, the image is segmented into foreground and background regions based on the threshold T_k, and the average grayscale values Z_B and Z_o of these two parts are calculated.

$$Z_o = \frac{\sum_{Z(i,j)<T_k} Z(i,j) \times N(i,j)}{\sum_{Z(i,j)<T_k} N(i,j)} \tag{7}$$

$$Z_B = \frac{\sum_{Z(i,j)>T_k} Z(i,j) \times N(i,j)}{\sum_{Z(i,j)>T_k} N(i,j)} \tag{8}$$

where $Z(i,j)$ is the value of the grey scale at position $(i.j)$ in the image, and $N(i,j)$ is the weighting coefficient applied to point $(i.j)$.

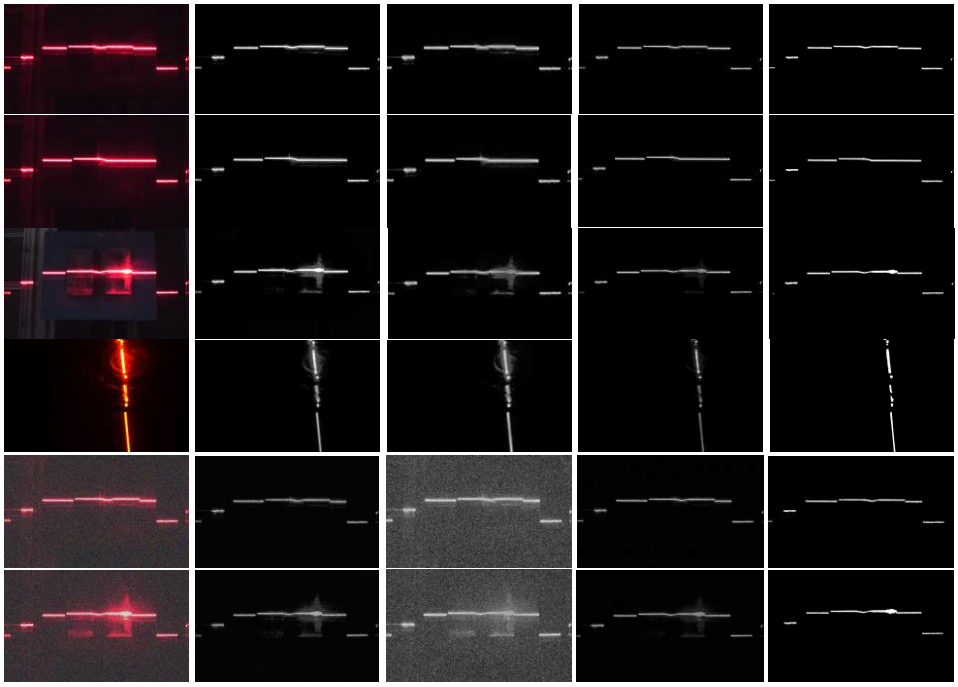
The above steps are repeated until the difference between T_k and the newly calculated threshold T_{k+1} is less than a predetermined parameter. The iteration ends, resulting in the optimal segmentation threshold T_{k+1}. The functional expression is as follows:

$$T_{k+1} = \frac{Z_o + Z_B}{2} \tag{9}$$

Compare the value of the grey scale of each pixel in the image with the threshold value. Pixels with values greater than T_{k+1} are classified as the target, while those with values less than T_{k+1} are classified as the background. That is:

$$g(i,j) = \begin{cases} 1, S(i,j) \geq T_{k+1} \\ 0, S(i,j) < T_{k+1} \end{cases} \tag{10}$$

The process of saliency feature fusion under different interference scenarios is illustrated in Fig.2. An Experimental analysis was conducted on various reflective scenarios, high noise, and laser speckle interference. The color distance saliency map effectively reduces complex background interference and accurately identifies the contour features of laser stripes. The local saliency map can focus on the overall distribution of the stripe features, highlighting the brightness characteristics of the laser stripes. The fused saliency map further filters background interference features without damaging the actual contour of the laser stripes, demonstrating that the proposed feature fusion algorithm is robust and accurate.



(a) Original image (b) Color distance saliency map (c) Local saliency map (d) Fused saliency map (e) Segmentation results

Fig 2 Saliency Feature Fusion Process.

2.2 Precise extraction of stripe center with secondary smoothing

Accurate laser stripe center extraction is critical to complete 3D feature extraction of welds in reflective scenes. To optimize and achieve smoother laser stripe extraction, this paper employs the Grey Gravity function to determine the initial center of the laser stripe and applies the Savitzky-Golay filter to smooth the initial laser stripe centerline, resulting in more fluid and consistent laser stripe extraction. The expression for the Gray-gravity function is:

$$x_o = \sum_{i=1}^{M}\sum_{j=1}^{N} i \cdot I(i,j) \Big/ \sum_{i=1}^{M}\sum_{j=1}^{N} I(i,j) \tag{11}$$

$$y_o = \sum_{i=1}^{M}\sum_{j=1}^{N} j \cdot I(i,j) \Big/ \sum_{i=1}^{M}\sum_{j=1}^{N} I(i,j) \tag{12}$$

where (x_o, y_o) is the stripe center coordinate and $I(i,j)$ represents the grayscale value at row i and column j of the image.

The Savitzky-Golay filter method[17], based on the principles of least squares and polynomial expansion, assumes a window width n (where n=2m+1). The initial laser stripe center position within the window is:

$$x = (-m, -m+1, \cdots, -1, 0, \cdots, m-1, m) \tag{13}$$

The initial stripe centerline within the window is fitted using a $k-1$ order polynomial as follows:

$$y = a_0 + a_1 x + a_2 x^2 + a_3 x^3 + \cdots + a_{k-1} x^{k-1} \tag{14}$$

Rewrite formula (14) in matrix form, and the functional expression is:

$$\begin{bmatrix} y_{-m} \\ y_{-m-1} \\ \vdots \\ y_m \end{bmatrix} = \begin{bmatrix} 1 & -m & \cdots & (-m)^{k-1} \\ 1 & -m+1 & \cdots & (-m+1)^{k-1} \\ \vdots & \vdots & \vdots & \vdots \\ 1 & m & \cdots & (m)^{k-1} \end{bmatrix} \begin{bmatrix} a_0 \\ a_1 \\ \vdots \\ a_{k-1} \end{bmatrix} + \begin{bmatrix} e_{-m} \\ e_{-m+1} \\ \vdots \\ e_m \end{bmatrix} \tag{15}$$

By abbreviating equation (15), the functional expression is:

$$Y_{(2m+1)\times 1} = X_{(2m+1)\times k} \cdot A_{k\times 1} + E_{(2m+1)\times 1} \tag{16}$$

where E is the value of the error between original strip center line and smoothed result. Therefore, the least squares solution of A can be calculated as:

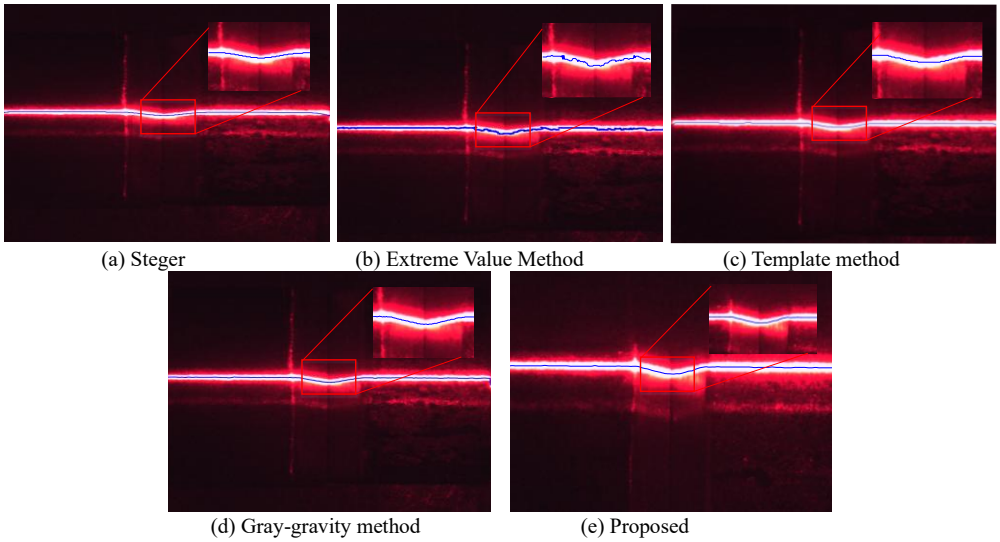
$$\hat{A} = (X^T \cdot X)^{-1} \cdot X^T \cdot Y \tag{17}$$

The final smoothed result Y is calculated as follows:

$$\hat{Y} = X \cdot A = X \cdot (X^T \cdot X)^{-1} \cdot X^T \cdot Y = B \cdot Y \tag{18}$$

where $B = X \cdot (X^T \cdot X)^{-1} \cdot X^T$.

Fig.3 illustrates the results of weld seam centerline extraction using various algorithms. By comparing the extremum method [18], Steger's algorithm [19], template method [20], and the Gray-gravity method [21], It is clear that, while all the mentioned algorithms are capable of accurately extracting the center of the laser stripe, Steger's method does not accurately extract the stripe center in areas with significant curvature changes. The extremum method exhibits substantial errors in regions with curvature changes. Although both the template method and the Grey Gravity function can accurately extract the stripe center, the resulting centerline is jagged and lack smoothness, requiring further refinement to enhance continuity. Fig.4 shows the running time for centerline extraction using different algorithms. From the figure, it can be seen that the extraction time for this method is 0.72 seconds, which is relatively fast.



(a) Steger (b) Extreme Value Method (c) Template method

(d) Gray-gravity method (e) Proposed

Fig. 3 Comparison of Different Centerline Extraction Algorithms

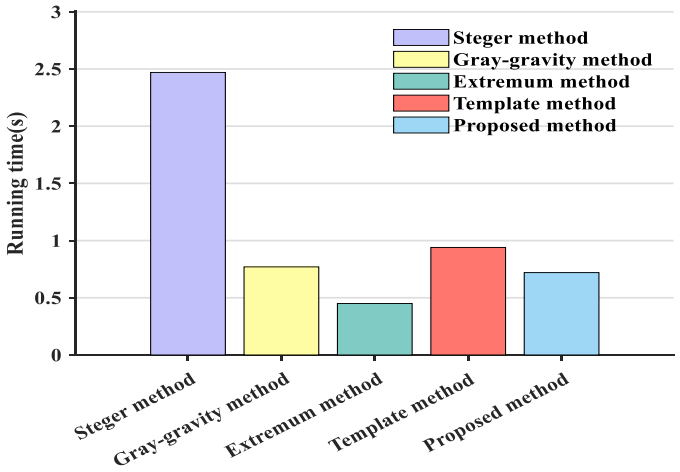
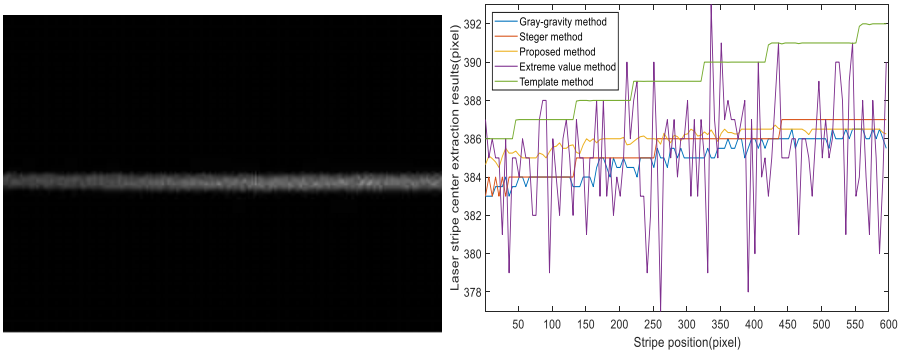


Fig. 4 Comparison of Running Time

As a further validation of the robustness of the presented algorithm for centerline detection, we tested the accuracy of the centerline detection output on a flat surface and under different noise backgrounds. Fig. 5 shows the centerline extraction results on a flat surface. According to Table 1, the proposed laser stripe center extraction algorithm exhibits good stability, with both low variance and standard deviation.



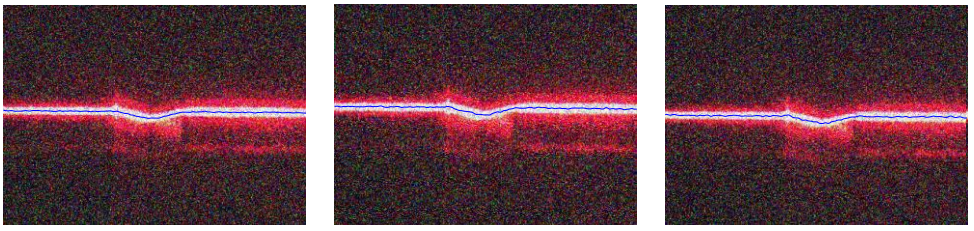
(a)Flat Laser Stripe (b) Comparison of Different Laser Stripe Centerlines

Fig. 5 Centerline Extraction Results on a Flat Surface

TABLE 1 RESULTS OF COMPARISON OF LASER STRIP CENTRE

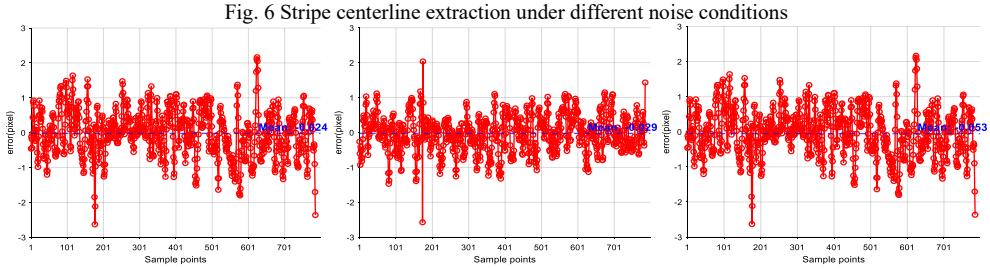
Method	Pixel mean value	Variance	Standard deviation
Steger method	385.0718	1.2750	1.1292
Gray-gravity method	385.5395	1.1083	1.0528
Template method	390.0796	9.3638	3.0600
Extreme value method	385.5276	9.9666	3.1573
Algorithm in this paper	386.0716	0.2498	0.4998

Fig. 6 displays the centerline extraction results under different noise conditions. Gaussian noise was added with a mean of 0 and variances of 0.1, 0.2 and 0.4, denoted Noise1, Noise2 and Noise3, respectively. It is evident from Fig. 6 that the proposed approach accurately extracts the laser stripe center under varying noise levels, demonstrating good robustness. Fig. 7 presents the error curve analysis results under different noise levels. Figs. 7(a)-(c) show the differences in the laser stripe center under Noise3 versus Noise2, Noise2 versus Noise1, and Noise3 versus Noise1, referred to as Error1, Error2, and Error3, respectively. Figure 7 shows that the error curves have minimal variations with mean errors of -0.024, -0.029 and -0.053 respectively. The experimental results demonstrate that the proposed centerline extraction methodology has a high level of precision and robustness under various noise interferences.



(a) Noise1 (b) Noise2 (c) Noise3

Fig. 6 Stripe centerline extraction under different noise conditions



(a) Error1 (b) Error 2 (c) Error 3

Fig. 7 Error curve analysis

2.3 Automatic extraction of weld trajectory

In this paper, the path of the welding seam is determined by applying a least squares fit to the feature points located at the lowest part of the V-groove weld seam. For the initial point cloud data $P_i(x_i,y_i)$, $(i=1,2,\cdots m)$, the function expression for the linear fitting of the weld seam path is as shown below:

$$y(x)=a+bx \tag{19}$$

where $y(x)$ is the reference line for fitting the weld seam，a and b are the coefficient to be fitted.

Let d_i be the spacing from the initial dot cloud data to the fitting line, and the function expression is:

$$d_i=y_i-(a+bx_i) \tag{20}$$

This paper uses the technique of least squares to find the best solution that minimizes the total quadratic discrepancies. The function expression is:

$$D = \sum_{i=1}^{m} d_i^2 = \sum_{i=1}^{m} (y_i - a - bx_i)^2 \tag{21}$$

Calculate the fractional differentiation of D regarding every value of the constant, where the function expression is:

$$\frac{\partial D}{\partial a} = -2\sum_{i=1}^{m} (y_i - a - bx_i) \tag{22}$$

$$\frac{\partial D}{\partial b} = -2\sum_{i=1}^{m} (x_i y_i - ax_i - bx_i^2) \tag{23}$$

The parameters to be fitted a and b can be found by making the partial derivatives zero, respectively.

$$a = \bar{y} - b\bar{x} \tag{24}$$

$$b = \frac{\sum_{i=1}^{m} (x_i - \bar{x})(y_i - \bar{y})}{\sum_{i=1}^{m} (x_i - \bar{x})^2} \tag{25}$$

Sample along the x-axis while applying constraints in the direction of the y-axis to determine the lowest point coordinates in each x-axis direction corresponding to the z-axis. The function expression for this process is:

$$dist_i = min(z_i) \tag{26}$$

Therefore, the standard deviation is set according to the distance d_i, and the function expression is:

$$\sigma = \sqrt{\frac{1}{m}\sum_{i=1}^{m} (dist_i - \overline{dist})^2} \tag{27}$$

where $\bar{d} = \frac{1}{m}\sum_{i=1}^{m} dist_i$, and σ is the standard variance.

According to the standard deviation for the rejection of the abnormal point cloud, if $dist_i \le 2\sigma$,it means that point P_i is a standard point, retain point P_i; if $dist_i > 2\sigma$, it means that point P_i is an anomaly, reject point P_i. Finally, based on the retained point P_i, a least squares fit is performed to obtain the final fitted line.

3 Analysis of results

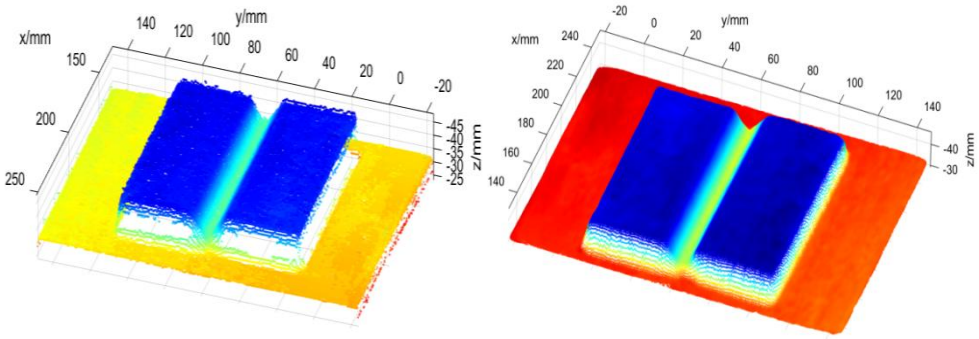
To verify the effectiveness and reliability of the calculation algorithm, 3D imaging tests were conducted on V-groove weld seam specimens, and the proposed algorithm was used

to extract the welding trajectory. The weld seam tracking system in the experiment consisted mainly of a CCD camera, a line laser emitter (with a wavelength of 650nm, width < 3mm, and output power of 500mw), and a six-degree-of-freedom robot. Figure 8 shows the system's imaging test screen, where active vision imaging was used to capture 3D images of the weld workpiece, obtaining 3D point cloud data. The imaging results are shown in Figure 9. From these figures, it is evident that the reconstruction results using the proposed method are smoother and more accurately reflect the precise 3D morphological characteristics of the measured workpiece.

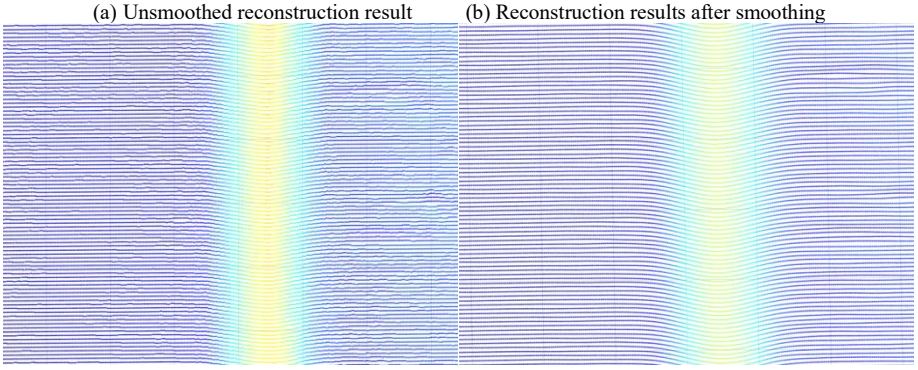


(a) experimental system (b) Weld testing

Fig. 8 System Imaging Platform



(a) Unsmoothed reconstruction result (b) Reconstruction results after smoothing

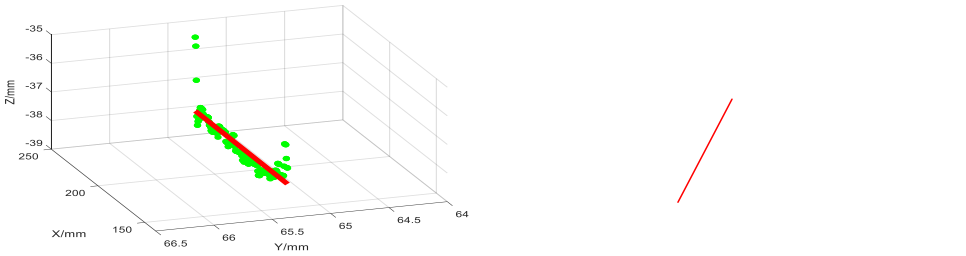


(c) Detail enlarged view before optimization (d) Detail enlarged view after optimization

Fig. 9 Weld seam 3D point cloud

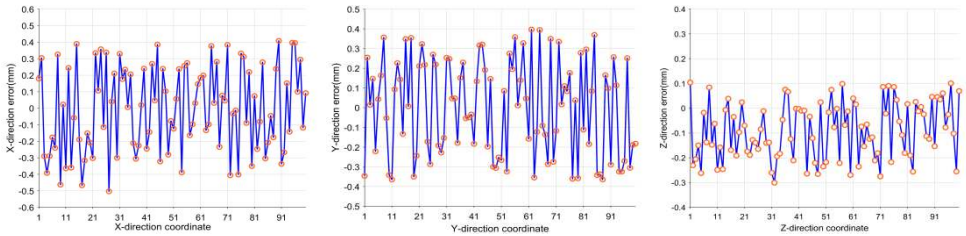
Fig. 10 shows the results of the extracted weld trajectory. The initial effective scatter plot data was fitted to derive the welding trajectory feature points, as illustrated in Fig.10(a). To evaluate the precision of the algorithm in extracting weld seam features, the start and end points of the weld trajectory were marked on the workpiece prior to the experiment, and these

coordinates were used as reference benchmarks. During the experiment, the fitted weld trajectory feature points were compared with the reference benchmark points. Fig. 11 displays the error curves in different directions. The curves indicate that the maximum error is 0.51mm in the X direction, 0.40mm in the Y direction and 0.29mm in the Z direction.



(a) Welding trajectory point cloud fitting (b) Welding trajectory extraction

Fig. 10 Welding trajectory extraction



(a) X-direction error (b) Y-direction error (c) Z-direction error

Fig. 11 Error curves

4 Conclusion

To achieve automatic extraction of weld trajectories, this research presents a methodology based on the fusion of salient features. First, a precise segmentation model is developed that utilizes saliency feature fusion techniques to accurately delineate the laser stripes at the weld seam and effectively reduce the interference caused by uneven illumination. Next, a Grey Gravity function based on Savitzky-Golay filtering is applied to retrieve the center of the laser stripes, enhancing the extraction accuracy. Finally, the smallest squares fitting algorithm is employed to automatically extract the welding trajectory. Experimental findings show that the presented approach successfully mitigates interference from reflections, with the largest fitting mistake of the weld trajectory being less than 0.51 mm.

Funding

Not applicable.

Declaration

We declare that we do not have any commercial or associative interest that represents a conflict of interest in connection with the work submitted.

References

[1] Kim, J., et al., Multiple weld seam extraction from RGB-depth images for automatic robotic welding via point cloud registration**[J]**. Multimedia Tools and Applications, 2021. 80(6): p. 9703-9719.DOI: https://doi.org/10.1007/s11042-020-10138-7.

[2] X, L., et al., Automatic Recognition of Multiple Weld Types Based on Structured Light Vision Sensor Using Deep Transfer Learning**[J]**. IEEE Sensors Journal, 2023. 23(7): p. 7142-7152.DOI: https://doi.org/10.1109/JSEN.2022.3224931.

[3] Yang, L., et al., A Novel 3-D Path Extraction Method for Arc Welding Robot Based on Stereo Structured Light Sensor**[J]**. IEEE Sensors Journal, 2019. 19(2): p. 763-773.DOI: https://doi.org/10.1109/JSEN.2018.2877976.

[4] Wu, Z., et al., Real-time segmentation network for accurate weld detection in large weldments**[J]**. Engineering Applications of Artificial Intelligence, 2023. 117: p. 105008.DOI: https://doi.org/10.1016/j.engappai.2022.105008.

[5] Xiao, R., et al., An adaptive feature extraction algorithm for multiple typical seam tracking based on vision sensor in robotic arc welding**[J]**. Sensors and Actuators A: Physical, 2019. 297: p. 111533.DOI: https://doi.org/10.1016/j.sna.2019.111533.

[6] X, L., et al., Feature Extraction of Welding Seam Image Based on Laser Vision**[J]**. IEEE Sensors Journal, 2018. 18(11): p. 4715-4724.DOI: https://doi.org/10.1109/JSEN.2018.2824660.

[7] Sung, K., et al., Development of a Multiline Laser Vision Sensor for Joint Tracking in Welding**[J]**. Welding Journal, 2009. 88(4): p. 79s-85s.

[8] He, Y., et al., Autonomous Detection of Weld Seam Profiles via a Model of Saliency-Based Visual Attention for Robotic Arc Welding**[J]**. Journal of Intelligent & Robotic Systems, 2016. 81(3): p. 395-406.DOI: https://doi.org/10.1007/s10846-015-0226-y.

[9] Banafian, N., R. Fesharakifard, and M.B. Menhaj, Precise seam tracking in robotic welding by an improved image processing approach**[J]**. The International Journal of Advanced Manufacturing Technology, 2021. 114(1): p. 251-270.DOI: https://doi.org/10.1007/s00170-021-06782-4.

[10] Fang, Z., et al., A Vision-Based Robotic Laser Welding System for Insulated Mugs with Fuzzy Seam Tracking Control**[J]**. Symmetry, 2019. 11(11).DOI:

https://doi.org/10.3390/sym11111385.

[11] Lu, J., et al., Plate additive, seam-tracking technology based on feature segmentation**[J]**. Optics & Laser Technology, 2024. 168: p. 109848.DOI: https://doi.org/10.1016/j.optlastec.2023.109848.

[12] Li, X., et al., Robust Welding Seam Tracking and Recognition**[J]**. IEEE Sensors Journal, 2017. 17(17): p. 5609-5617.DOI: https://doi.org/10.1109/JSEN.2017.2730280.

[13] Ye, C., et al., A Method of Binocular Laser 3-D Scanning Imaging for Reflective Workpieces**[J]**. IEEE Sensors Journal, 2023. 23(13): p. 15188-15198.DOI: https://doi.org/10.1109/JSEN.2023.3279855.

[14] Yuankai, Z., et al., A point cloud-based welding trajectory planning method for plane welds**[J]**. The International Journal of Advanced Manufacturing Technology, 2023. 125(3): p. 1645-1659.DOI: https://doi.org/10.1007/s00170-022-10699-x.

[15] Zhang, Y., et al., A Feature Extraction Approach Over Workpiece Point Clouds for Robotic Welding**[J]**. IEEE Transactions on Automation Science and Engineering, 2023: p. 1-10.DOI: https://doi.org/10.1109/TASE.2023.3345868.

[16] Liu, C., & Pang, M. (2020). Automatic lung segmentation based on image decomposition and wavelet transform. Biomedical Signal Processing and Control, 61, 102032. https://doi.org/10.1016/j.bspc.2020.102032

[17] John, A., J. Sadasivan, and C.S. Seelamantula, Adaptive Savitzky-Golay Filtering in Non-Gaussian Noise**[J]**. IEEE Transactions on Signal Processing, 2021. 69: p. 5021-5036.DOI: https://doi.org/10.1109/TSP.2021.3106450.

[18] Yuehua LI, J.Z., Lijian LIU, Research progress of line structured light measurement technology**[J]**. Journal of Hebei University of Science and Technology, 2018. 39(2): p. 115 – 124.DOI: https://doi.org/10.7535/hbkd.2018yx02004.

[19] Steger, C., An unbiased detector of curvilinear structures**[J]**. IEEE Transactions on Pattern Analysis and Machine Intelligence, 1998. 20(2): p. 113-125.DOI: https://doi.org/10.1109/34.659930.

[20] Hu, B., et al., New method for obtaining the center of structured light stripe by direction template**[J]**. Computer Engineering and Applications, 2002. 38(11): p. 59-60.DOI: https://doi.org/10.1007/BF02960786.

[21] Wu, X., et al., A novel high precise laser 3D profile scanning method with flexible calibration**[J]**. Optics and Lasers in Engineering, 2020. 132: p. 105938.DOI: https://doi.org/10.1016/j.optlaseng.2019.105938.